The ubiquitin-like (UBX)-domain-containing protein Ubx2/Ubxd8 regulates lipid droplet homeostasis

Chao-Wen Wang* and Shu-Chuan Lee

Institute of Plant and Microbial Biology, Academia Sinica, Nankang, Taipei 11529, Taiwan

*Author for correspondence (cwwang02@gate.sinica.edu.tw)

Accepted 20 February 2012
Journal of Cell Science 125, 2930–2939

doi: 10.1242/jcs.100230

Summary

Lipid droplets (LDs) are central organelles for maintaining lipid homeostasis. However, how cells control the size and number of LDs remains largely unknown. Herein, we report that Ubx2, a UBX-domain-containing protein involved in endoplasmic reticulum (ER)-associated degradation, is crucial for LD maintenance. Ubx2 redistributes from the ER to LDs when LDs start to form and enlarge during diauxic shift and in the stationary phase. *ubx2Δ* cells contain abnormal numbers of LDs that are smaller than normal, and their triacylglycerol (TAG) is reduced to 50% of the normal level. Deletion of either the UBX or UBA domain in Ubx2 has no effect, but deletion of both causes LD phenotypes similar to that in *ubx2Δ*. The reduced level of TAG in *ubx2Δ* is probably the result of mislocalization of phospholipid:diacylglycerol acyltransferase (Lro1), one of the two TAG-synthesizing enzymes in yeast, which moves along the ER and distributes dynamically to the putative LD assembly sites abutting LDs. Thus, Ubx2 is important for the maintenance of cellular TAG homeostasis probably through Lro1. The mammalian Ubxd8 (also known as FAF2), when expressed in yeast, complements the defect of *ubx2Δ*, implying a functional conservation for these UBX-domain-containing proteins in lipid homeostasis.

Key words: Endoplasmic reticulum, ER, Lipid droplets, Triacylglycerol, Ubx2, Lro1, ERAD, ER-associated degradation

Introduction

In eukaryotic cells, lipid droplets (LDs) are the major organelles for the storage of neutral lipids, including triacylglycerol (TAG) and sterol ester (SE). LDs contain a central neutral lipid core that is surrounded by a phospholipid monolayer. Many human metabolic diseases, such as obesity, diabetes and atherosclerosis, are linked to LD homeostasis (Krauss, 1998). LDs are not only important for lipid storage, but also for maintaining lipid homeostasis and protein management (Farese and Walther, 2009; Goodman, 2008; Walther and Farese, 2009).

LDs associate with endoplasmic reticulum (ER), mitochondria, peroxisomes, vacuoles and lysosomes, suggesting their interplay in lipid metabolism (Blanchette-Mackie et al., 1995; Novikoff et al., 1980). LDs are thought to emerge from the ER (Walther and Farese, 2009). During biogenesis, neutral-lipid-synthesizing enzymes generate lenses of neutral lipids that then bulge from the outer leaflet of ER. Indeed, recent studies in yeast have proved that LDs are absent in cells that cannot synthesize neutral lipids (Garbarino and Sturley, 2005; Sorger et al., 2004), highlighting the importance of neutral-lipid-synthesizing enzymes during LD biogenesis.

In mammals, cellular TAG and SE synthesis are catalyzed by the products of the acyltransferase gene families, which include acyl-CoA:cholesterol O-acyltransferase (ACAT) and lecithin cholesterol acyltransferase (LCAT) for SE formation (Farese, 1998; Jonas, 2000); and acyl-CoA:diacylglycerol O-acyltransferase (DGAT) and phospholipid:diacylglycerol O-acyltransferase (PDAT) for TAG formation (Yen et al., 2008). Similar mechanisms are also present in the budding yeast *Saccharomyces cerevisiae* (Rajakumari et al., 2008). The ACAT-related enzymes Are1 and Are2 reside in ER and mediate the esterification step for SE synthesis in yeast (Oelkers et al., 1998; Yang et al., 1996). TAG synthesis in most cells, including yeast, occurs by the Kennedy pathway that involves multiple enzymatic reactions in different organelles, including ER, mitochondria and LDs. An important precursor for TAG formation is phosphatidic acid (PA), which also serves as the major precursor for the phospholipid biosynthetic pathways. PA is dephosphorylated by PA phosphatase, lipin in mammals and Pah1 in yeast, to yield diacylglycerol (DAG) (Adeyo et al., 2011). The last step for TAG formation is catalyzed by Dga1 (Oelkers et al., 1998). Dga1 exerts its enzymatic function mainly in the ER and LDs (Sorger and Daum, 2002), although its mammalian homolog DGAT2 was also found in mitochondria (Stone et al., 2009). In addition, the yeast PDAT homolog Lro1 synthesizes another pool of TAG in yeast (Oelkers et al., 2000). Unlike Dga1, which uses DAG as a substrate for TAG synthesis, Lro1 catalyzes phosphatidylcholine-dependent TAG formation (Dahlqvist et al., 2000), and thereby is considered to have a role in membrane lipid modification. However, how the synthesized TAG and SE reach LDs remains an open question.

The biogenesis and regression of LDs probably involve integral membrane proteins that mark the phospholipid monolayer. Genome-wide searches for LD mutants and LD proteomes in several systems such as yeast (Athenstaedt et al., 1999; Fei, et al., 2008; Szymanski, et al., 2008), fly (Beller et al., 2006; Beller et al., 2008; Guo et al., 2008) and mammals (Brasaemle et al., 2004; Fujimoto et al., 2004) have identified dozens of proteins. The LD structural proteins might regulate lipolysis (Londos et al., 2005; Sztalryd et al., 2003), sequestration of newly synthesized lipids to facilitate LD maturation, and lipid trafficking (Fujimoto et al., 2001; Fujimoto et al., 2004; van Meer, 2001). In contrast to the mammalian system, the LD

proteome of budding yeast suggests that the majority of LD-localized proteins are enzymes involved in lipid metabolism (Athenstaedt et al., 1999). These include Erg1, Erg6 and Erg7 for ergosterol biosynthesis; Faa1, Faa4 and Fat1 for fatty acid metabolism; and Tgl1, Tgl3, Tgl4 for neutral lipid degradation (Athenstaedt et al., 1999). It is unclear whether these enzymes in yeast also have structural roles or there exist additional LD structural proteins that are yet to be identified.

Ubx2 is a transmembrane protein localized to ER (Schuberth and Buchberger, 2005). It is well known to be part of the quality control mechanisms that selectively transport the terminally misfolded proteins from the ER to the cytosol for subsequent ubiquitylation and proteasomal degradation, a process called ER-associated degradation (ERAD) (Römisch, 2006). During ERAD, Ubx2 functions to bridge the cytosolic Cdc48–Npl4–Ufd1 complex and the membrane-associated Hrd1–Hrd3 and Ssm4 ubiquitin ligase complexes using its N-terminal ubiquitin-associated (UBA) domain to recognize the ubiquitylated ERAD substrates, and its C-terminal UBX domain to interact with the Cdc48–Nple–Ufd1 complex (Neuber et al., 2005; Schuberth and Buchberger, 2005; Schuberth et al., 2004). Ubxd8 (also known as FAF2) is one of the close homologs of Ubx2 in mammals. It has been identified as a ERAD component for dislocation of class I major histocompatibility complex heavy chain (Mueller et al., 2008), and is required for Insig-1 degradation by ERAD in fatty-acid-depleted cells (Lee et al., 2008). Interestingly, Ubxd8 has been found in a mammalian LD proteome (Zehmer et al., 2009; Zehmer et al., 2008), and is implicated in TAG metabolism by blocking the conversion of DAG to TAG in culture cells depleted of fatty acids (Lee et al., 2010).

In this study, we report a previously unknown function of Ubx2 in maintaining LD homeostasis. Our data reveal that Ubx2 localizes to the ER and LDs. Cells either lacking or overproducing Ubx2 show aberrant LD morphology. One of the defects in *ubx2Δ* is reduced TAG level, which might be linked to the mislocalized Lro1. The defects in *ubx2Δ* could be complemented by mammalian Ubxd8, suggesting a functional conservation.

Results

Ubx2 localizes to the lipid droplets

Ubx2, a previously characterized ER protein, is known to function in bridging the substrate-recognition machinery and the Cdc48–Npl4–Ufd1 dislocation complex during ERAD (Neuber et al., 2005; Schuberth and Buchberger, 2005; Schuberth et al., 2004). Most fluorescently tagged ER proteins, such as Sec63–mCherry, show classic perinuclear and cortical ER localization (Fig. 1A). Although Ubx2–GFP showed perinuclear ER localization, it also appeared as reticular structures near the cell periphery that colocalized with the mitochondrial marker Su9–mCherry but not with Sec63–mCherry in log phase (Fig. 1A). Intriguingly, unlike most ER proteins that stay on the ER, Ubx2–GFP relocalized to ring structures next to the ER when cells were grown to diauxic shift (Fig. 1A), a condition in which nutrients become limited and LD biogenesis is activated. We show that the ring structures of Ubx2 were colocalized with the LD marker

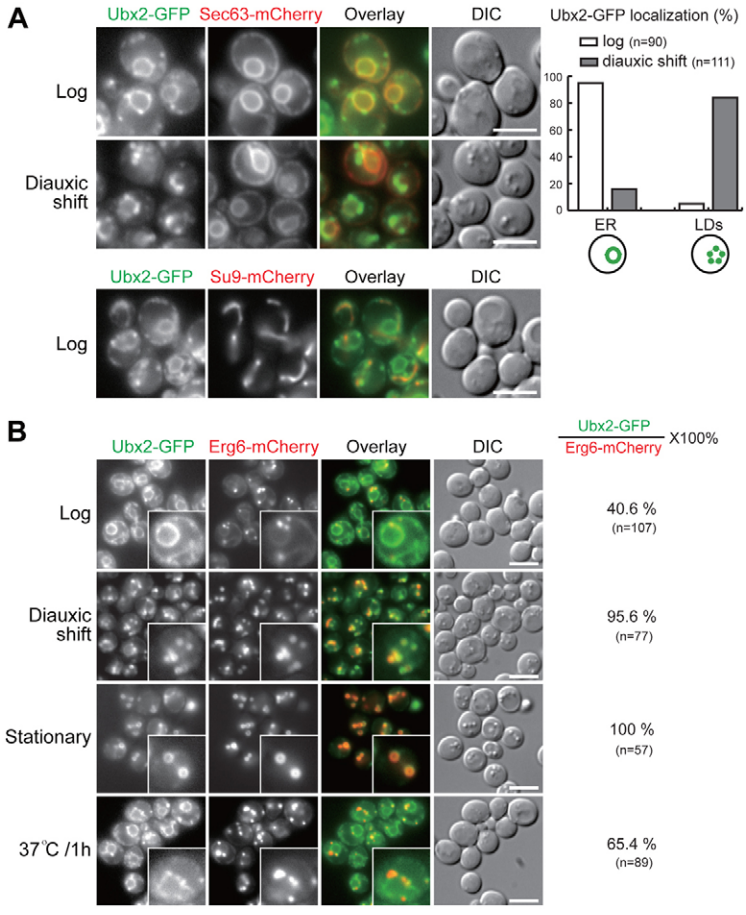

Fig. 1. Ubx2 dynamically localizes to ER, LDs and mitochondria. (**A**) Yeast cells expressing Ubx2–GFP and Sec63–mCherry or Su9–mCherry were grown to the stages as indicated and then examined by fluorescence microscopy. The percentage of Ubx2–GFP localized to the ER or LDs and the number of cells counted (n) are shown in the bar chart. (**B**) Yeast cells expressing Ubx2–GFP and Erg6–mCherry were grown to various stages as indicated and then examined by fluorescence microscopy. The inset in each image shows a higher magnification view of a cell. The percentage of Ubx2–GFP associated with LDs (marked by Erg6–mCherry) and the number of cells counted (n) are also shown. Scale bars: 5 μm.

Erg6–mCherry (Fig. 1B). As the LDs enlarge during the stationary phase, the rings of Ubx2–GFP became evident (Fig. 1B). The association of Ubx2 with nascent LDs as determined by the percentage of Ubx2–GFP colocalization with LD marker Erg6–mCherry was also found in a LD-induction condition in which the log phase culture was shifted to 37℃ for 1 hour (Fig. 1B). Thus, we conclude that Ubx2 is a very dynamic protein, probably shuttling between ER, LDs and mitochondria, implying a complicated functional network for Ubx2.

Ubx2 functions independently of ERAD in LDs

The LD localization of Ubx2 appeared to correlate well with LD formation. To test whether Ubx2 might have a role on LDs, we generated a *ubx2Δ* strain and stained the cells with Bodipy 493/503, a lipophilic dye that specifically recognizes neutral lipids. Unlike wild-type cells that accumulated LDs of fairly uniform size and number, the LDs in *ubx2Δ* cells were heterogeneous (Fig. 2A). Some *ubx2Δ* cells accumulated a large number, whereas the majority contained a few or even no LDs (Fig. 2B). LD size in *ubx2Δ* cells was reduced to ~50% of the average wild-type LD volume in most conditions examined (Fig. 2C). Furthermore, the abundant LD proteins Erg1 and Erg6 redistributed back to ER in *ubx2Δ* (Fig. 2D), similar to those yeast mutants known to be defective in LD biogenesis (Sorger et al., 2004). Consistent with the in vivo observations (Fig. 2A–C), purified LDs from *ubx2Δ* were smaller and less stained with Bodipy than those in the wild-type cells (Fig. 2E). We examined several abundant LD proteins by immunoblotting and found that Erg6 and Pet10 levels in *ubx2Δ* LDs were much reduced, in contrast to Erg1 and Ayr1 that remained the same (Fig. 2E). Thus, lack of *ubx2* caused aberrant morphology and protein composition in LDs. However, it remains unclear whether these two phenotypes are related.

LDs in various ERAD mutants are relatively homogeneous, similar to that in the wild type (data not shown). *cue1Δ* and *ubc7Δ* cells accumulated even more LDs than the wild type (supplementary material Fig. S2A). In addition, *ubx2Δ* cells died quickly in starvation, probably as a consequence of lipid metabolism defect, whereas most ERAD mutants survived as well as the wild type (supplementary material Fig. S2B). Furthermore, none of these ERAD components localized to LDs even in the stationary phase (data not shown). Cdc48, Npl4 and Ufd1 are essential for growth, and form the dislocation complex for ERAD. The LD-localized Ubx2–GFP did not correlate with the localization of mCherry-tagged Cdc48, Npl4 or Ufd1 (supplementary material Fig. S2C). In addition, the LD morphology did not change when *cdc48-3*, *npl4-1* and *ufd1-2* were shifted from room temperature to a nonpermissive temperature of 33℃ for 3 hours, and none of the mutants showed smaller or heterogeneous LDs similar to *ubx2Δ* cells (supplementary material Fig. S2D). Thus, these data imply that Ubx2 might exert additional functions on LDs, probably independent of its known ERAD activities.

The UBA and UBX domains cooperate for Ubx2 function

A series of deletion constructs were made to further understand the role of Ubx2 on LDs. Deletions of the first 120 residues containing the known UBA domain or those after 410 containing the known UBX domain did not cause LD defects (Fig. 3A). To confirm these observations, we integrated *UBX2* variants into the genome of *ubx2Δ* cells (supplementary material Fig. S1) and examined their activities for ERAD and LD maintenance. The

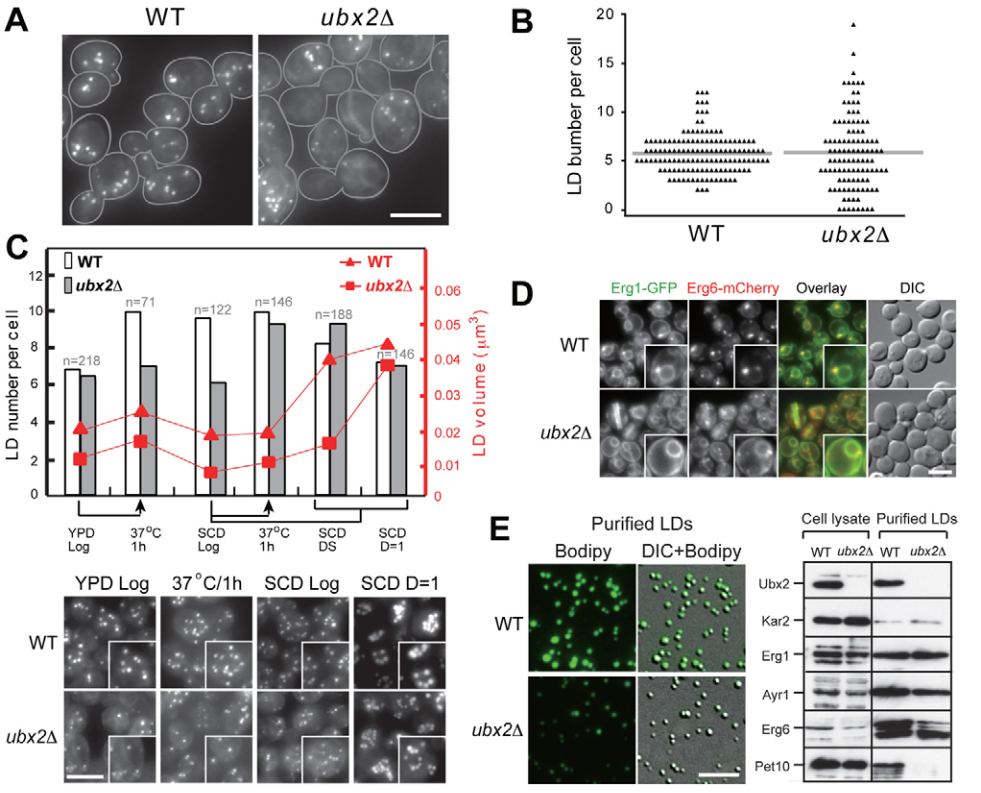

Fig. 2. The *ubx2Δ* cells accumulate aberrant LDs. (**A**) The LDs in wild-type (WT) and *ubx2Δ* cells were stained with Bodipy for fluorescence microscopy. Images were processed using deconvolution and maximal projection; cell shapes were outlined. (**B**) A scatter plot of the number of LDs in 100 cells as in A. (**C**) The number (black axis) and size (red axis) of LDs in wild-type and *ubx2Δ* cells grown in the conditions indicated. n, the number of cells quantified at each stage. Images of LDs in cells grown in various conditions are shown below; insets in each image shows a higher magnification of the LDs. (**D**) Wild-type and *ubx2Δ* cells expressing Erg1–GFP and Erg6–mCherry were imaged by fluorescence microscopy, and the insets show a higher magnification view of the cell. (**E**) The purified LDs from wild-type and *ubx2Δ* strains were stained with Bodipy for fluorescence microscopy (left). (Right) The abundance of proteins in total cell lysates or purified LDs from wild-type and *ubx2Δ* strains were compared by immunoblotting using anti-Ubx2, -Kar2, -Erg1, -Ayr1, -Erg6 and -Pet10 antibodies. Kar2 is an ER luminal protein, which served as a control for ER contamination. Scale bars: 5 μm.

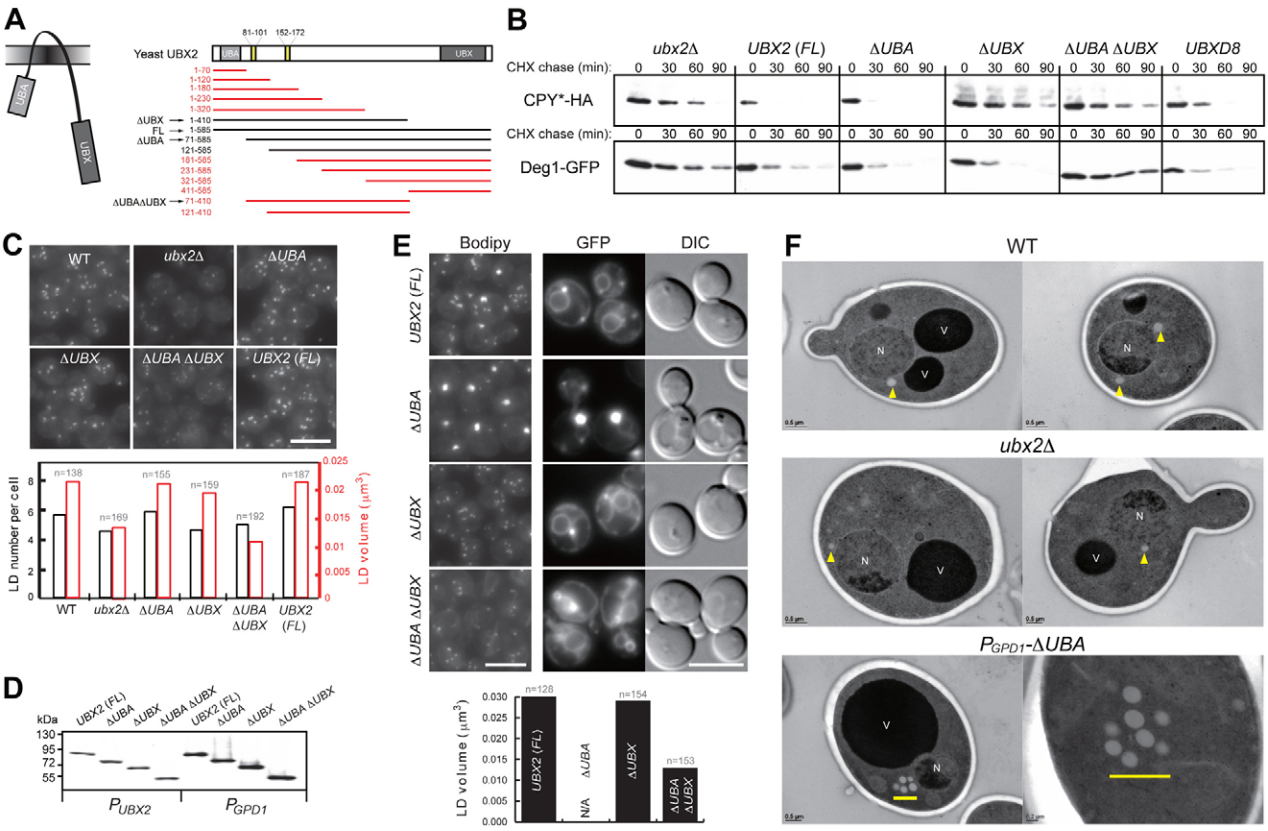

Fig. 3. The roles of the UBX and UBA domains within Ubx2 in LD maintenance and ERAD. (**A**) The topology of Ubx2 on the membrane and the diagram of domains and transmembrane regions (yellow) in Ubx2. The *ubx2Δ* cells transformed with the indicated Ubx2 variants resulted in normal (black, wild-type-like) or altered (red, *ubx2Δ*-like) LDs. (**B**) The *ubx2Δ*, Ubx2 variants expressed from the endogenous promoter, and P_{GPD1}-Ubxd8 strains expressing CPY*–HA or Deg1–GFP were treated with cyclohexamide (CHX; 1 mg/ml). Samples from the indicated chase time points were analyzed by western blot with anti-HA or anti-GFP antibodies. (**C**) The LDs in wild type, *ubx2Δ* and *ubx2Δ* cells expressing Ubx2 variants from the endogenous promoter were imaged during log phase. The number of LDs (black axis) and their size (red axis) are shown below. n, the number of cells quantified. (**D**) Various strains expressing endogenous (P_{UBX2}, black) or overproduced (P_{GPD1}, red) protein-A-tagged Ubx2 variants were compared for their protein level by western blot with anti-PrA antibody. P_{GPD1} samples were loaded with 10-fold dilution. (**E**) (Bodipy) The LDs in *ubx2Δ* cells expressing the indicated Ubx2 variants from the P_{GPD1} promoter were imaged in log phase. (GFP and DIC) Cells expressing the indicated GFP-tagged Ubx2 variants from the P_{GPD1} promoter were imaged in log phase. LD size is also shown (below), except for cells expressing *UBA*-truncated *UBX2* (*ΔUBA*) that formed aggregated LDs. n, the number of cells quantified. (**F**) Electron micrographs of wild-type, *ubx2Δ* cells and cells expressing *ΔUBA* from the P_{GPD1} promoter. Yellow arrowheads and yellow lines denote the scattered and aggregated LDs, respectively. N, nucleus. V, vacuole. Scale bars: 5 μm (C,E) and 0.5 μm (F).

misfolded carboxypeptidase Y (CPY*)-HA, a model substrate for ERAD, was stabilized in *ubx2Δ* cells expressing UBX-truncated Ubx2 (Fig. 3B), consistent with the previous results (Schuberth and Buchberger, 2005). However, LD morphology in this mutant was similar to that in the wild type (Fig. 3C). Although the UBA domain had been implicated in ERAD, the mutant showed a similar turnover rate of CPY*–HA as in the wild type (Fig. 3C). In cells expressing Ubx2 lacking both UBX and UBA domains, both ERAD substrates CPY*-HA and Deg1–GFP were stabilized and LD morphology was altered, similar to that in *ubx2Δ* (Fig. 3B,C). Thus, the two domains within Ubx2 probably act closely during ERAD and LD maintenance.

We further generated yeast strains overexpressing various Ubx2 variants through the strong *GPD1* promoter. Western blot results showed that all of proteins were expressed more than twentyfold that of the endogenous protein (Fig. 3D). LDs in cells overexpressing full-length (FL), UBA-truncated (*Δ*UBA) and UBX-truncated (*Δ*UBX) Ubx2 were prone to aggregate during diauxic shift and in stationary phase (data not shown). Extensive LD aggregation could be easily detected in cells overexpressing Ubx2 even in log phase (Fig. 3E,F). Unlike Ubx2 (FL)–GFP and Ubx2 (*Δ*UBX)–GFP that localized to both ER and LDs, Ubx2 (*Δ*UBA)–GFP clustered on the LDs but not ER (Fig. 3E). Thus, Ubx2 (*Δ*UBA) might prefer LDs or fail to exit from LDs. Importantly, it suggests that strong association of Ubx2 with LDs could result in LD aggregation. Using thin-section electron microscopy, we confirmed that *ubx2Δ* cells contained smaller LDs. By contrast, cells overexpressing UBA-truncated Ubx2 showed LD clustering to form aggregates (Fig. 3F).

By contrast, Ubx2 (*Δ*UBX*Δ*UBA) overexpression caused LD phenotypes similar to that in *ubx2Δ*. Ubx2 (*Δ*UBX*Δ*UBA)–GFP at the endogenous or higher level localized to the ER and mitochondria but not LDs (Fig. 3E), even though a substantial number of small LDs were indeed formed in these strains. Thus, a failure of partitioning Ubx2 into LDs, such as in *ubx2Δ* or in cells expressing Ubx2 (*Δ*UBX*Δ*UBA) correlated well with small and

heterogeneous LD morphology. Together, these results are consistent with a model in which the amount and location of Ubx2 is crucial for maintaining the basic structure of LDs.

ubx2Δ causes Lro1 mislocalization

Our data have established that the association of Ubx2 with LDs is crucial for LD maintenance. Because LD formation requires neutral lipid production, we tested the possibility that Ubx2 regulates this process. Lipid analysis showed that *ubx2Δ* cells accumulated ~50% TAG and an increased level of SE compared with the wild-type cells (Fig. 4A). The reduction of TAG appeared to correlate well with the LD defect in various *ubx2* mutants examined (supplementary material Fig. S3). TAG in yeast is produced from DAG by two major acyltransferases, TAG-synthesizing enzymes Dga1 and Lro1 (Sorger and Daum, 2002). Comparison of these two proteins at their steady state showed that *ubx2Δ* cells accumulated slightly more Lro1–13Myc than the wild-type cells (Fig. 4B). Although cyclohexamide chase experiment indicated that Lro1–13Myc is a short-lived protein (Fig. 4C), the stability of Lro1–13Myc was unaffected in *ubx2Δ* cells. Thus, Lro1 is probably not an ERAD substrate that requires Ubx2 for degradation.

To better understand the regulation of the two TAG-synthesizing enzymes at the cellular level, we generated strains expressing Dga1–mCherry and Lro1–mCherry and examined their association with LDs. Both fusion proteins are functional because Dga1–mCherry or Lro1–mCherry was sufficient to produce neutral lipids and form LDs when present as the sole enzyme of neutral lipid synthesis in the cells (Fig. 4D). Both proteins in log-phase cells were not readily detectable by fluorescence microscopy (data not shown). Upon diauxic shift, Dga1–mCherry localized to LDs, whereas Lro1–mCherry appeared as foci (Fig. 4E). The different localization pattern suggests their different roles in regulating neutral lipid productions and/or LD formation. Notably, each cell contained only one Lro1–mCherry focus that was often found in close proximity to LD markers such as Ubx2 and Tgl3 (Fig. 4F). The localization is reminiscent of the LD assembly site marked by Nem1, a protein that activates Pah1 (lipin in mammals) by recruiting Pah1 to the ER for DAG production (Adeyo et al.,

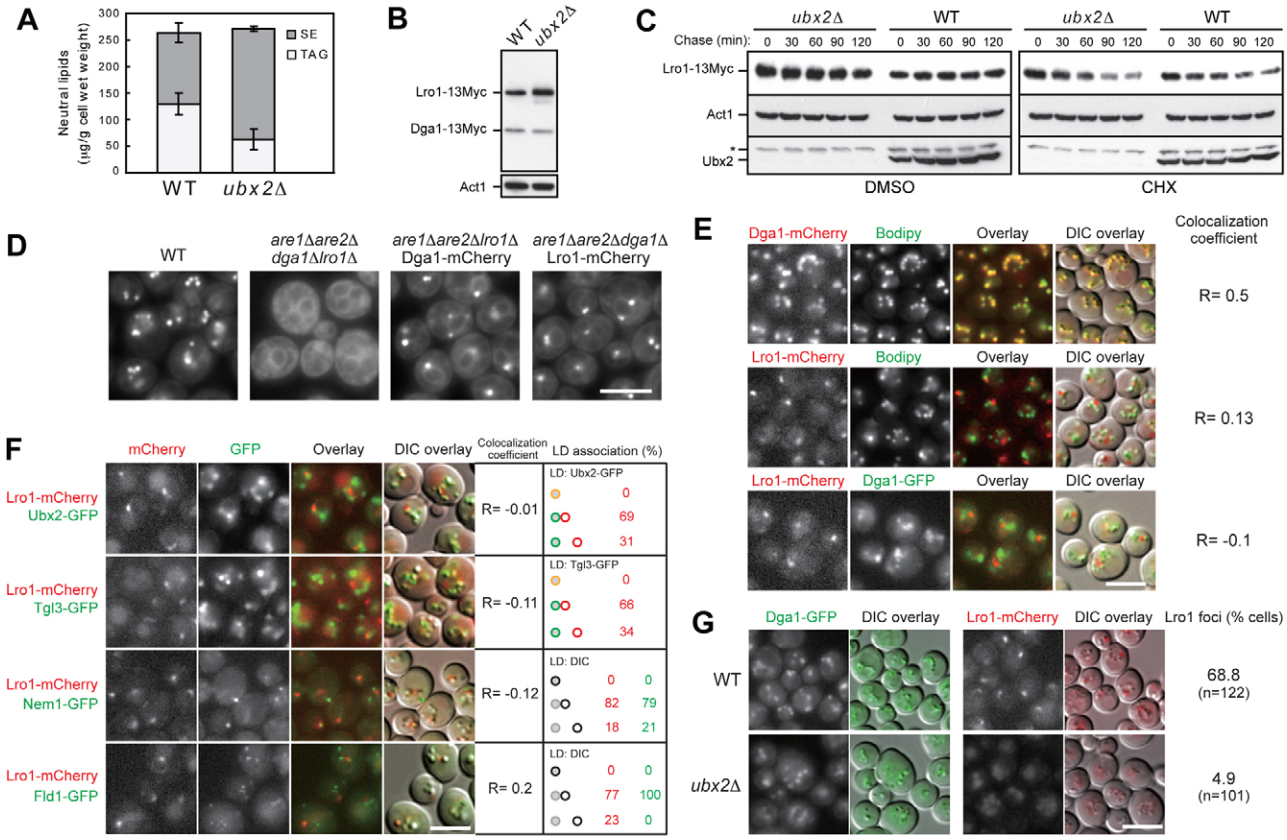

Fig. 4. The *ubx2Δ* cells show reduced TAG and mislocalized Lro1. (**A**) The total TAG and SE in wild-type and *ubx2Δ* cells were quantified, and the average from four independent experiments is plotted as means ± s.e.m. (**B**) Lro1–13Myc and Dga1–13Myc in wild-type and *ubx2Δ* cells were analyzed by western blotting with anti-Myc and anti-Act1 antibodies. (**C**) Yeast cells expressing Lro1–13Myc as indicated were treated with DMSO or cyclohexamide (CHX) and samples were analyzed by western blotting with anti-Myc, -Act1 and -Ubx2 antibodies. (**D**) Yeast strains as indicated were grown in YPD to diauxic shift and stained with Bodipy for fluorescence microscopy. (**E**) Yeast cells expressing the indicated proteins or with their LDs stained with Bodipy were imaged during diauxic shift in SCD. The colocalization coefficients (R) are shown. (**F**) Yeast cells expressing the indicated proteins were imaged during diauxic shift in SCD. The colocalization coefficients (R) for GFP and mCherry are shown. The percentage of LD association was determined by the positions of indicated GFP or mCherry fusion protein relative to the LDs that were marked by Ubx2–GFP or Tgl3–GFP, or determined by DIC imaging. $n>85$ cells. (**G**) Images of Dga1–GFP and Lro1–mCherry in wild-type and *ubx2Δ* cells during diauxic shift in SCD. The percentage of cells with Lro1–mCherry foci is shown. n, the number of cells quantified. Scale bars: 5 μm.

2011). The yeast seipin protein Fld1 also localized to the specific subdomain at the ER–LD contact sites (Szymanski, et al., 2008). However, Lro1–mCherry did not colocalize with Nem1–GFP and only partially overlapped with Fld1 (Fig. 4F). Thus, they appear to reside on different ER–LD subdomains or LD assembly sites. Intriguingly, very few Lro1–mCherry foci were found in *ubx2Δ* cells, although Dga1 localization was not affected (Fig. 4G). Similar results were also seen in the strains expressing Ubx2 without both UBA and UBX domains (data not shown). Because the protein level was not reduced (Fig. 4B), Lro1 is probably mislocalized in *ubx2Δ* cells.

To further understand the nature of Lro1 during LD dynamics, we checked the colocalization of Lro1–mCherry with various endomembrane markers, including the ER marker Sec63–GFP, peroxisomal marker GFP-SKL and mitochondrial marker Su9–GFP. We found that Lro1–mCherry localized within a specific region in the perinuclear ER (100%) and only a few foci (less than 5%) made contact with peroxisomes or mitochondria (Fig. 5A). Interestingly, when examined by time-lapse microscopy, Lro1–mCherry signals appeared to shuttle back and forth between LDs (supplementary material Movie 1). Biochemical fractionation assays revealed that Lro1 could be fully removed, by detergent, from the P13-enriched fraction of the ER (Fig. 5B). Thus, we conclude that Lro1 is probably an integral membrane protein in the ER and requires Ubx2 activity to form dynamic foci that travel along the ER to make contact with LDs.

Because Ubx2 is required for localization of Lro1 to the foci abutting LDs, we asked whether Ubx2 might control this activity through direct binding with Lro1. By using IgG–Sepharose to pull down Ubx2 with a protein A tag, we confirmed that Ubx2 binds strongly with Cdc48 as reported previously (Neuber et al., 2005; Schuberth and Buchberger, 2005; Schuberth et al., 2004), but not with Lro1–mCherry or Dga1–mCherry (Fig. 5C). We also did not detect specific interactions between Ubx2 and Erg6 or Pet10 (Fig. 5C), although both proteins seem to require Ubx2 for LD association (Fig. 2E). Thus, the recruitment of Lro1 to the dynamic foci and the arrangement of several proteins on LDs are probably controlled indirectly by the association of Ubx2 with LDs.

It is known that either Lro1 or Dga1 is sufficient for the biogenesis of LDs (Sorger et al., 2004). To test the hypothesis that Ubx2 affects Lro1 but not Dga1 activity to regulate a subset of TAG production and LD formation, we generated an *are1Δare2Δdga1Δubx2Δ* strain expressing Lro1 as the only acyltransferase for neutral lipid production and an *are1Δare2Δlro1Δubx2Δ* strain expressing only Dga1. If Lro1 mislocalization in the *ubx2Δ* strain resulted in the LD biogenesis defect, we suspected that the *are1Δare2Δdga1Δubx2Δ* strain should exhibit an LD-deficient phenotype similar to that of the *are1Δare2Δdga1ΔlroΔ* mutant, whereas the *are1Δare2Δlro1Δubx2Δ* strain would not. Indeed, we found that the *are1Δare2Δdga1Δubx2Δ* strain was deficient in LD formation even though Lro1 was present, whereas LDs were intact in the *are1Δare2Δdga1ΔlroΔ ubx2* strain (Fig. 5D). Together, our results indicate that the positioning of Lro1 is crucial for its functions during LD biogenesis and that Ubx2 serves as an important factor in regulating the process.

The mammalian Ubxd8 rescues the defects in *ubx2Δ*

In mammalian cells, the UBX-domain-containing protein Ubxd8 traffics from the ER to the LDs, reminiscent of Ubx2 localization

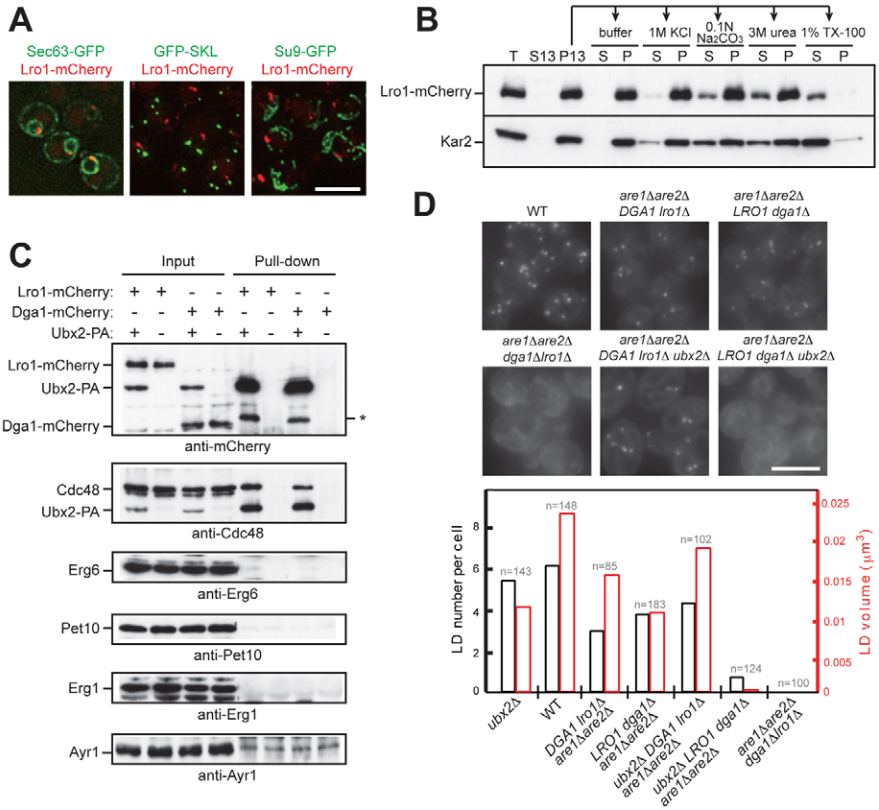

Fig. 5. Ubx2 regulates Lro1 but not Dga1 activity through an indirect mechanism. (**A**) Yeast cells expressing Lro1–mCherry and the ER marker Sec63–GFP, peroxisome marker GFP–SKL or mitochondria marker Su9–GFP were imaged by Z-section followed by deconvolution. The Lro1–mCherry and Sec63–GFP image is from one section, and the other two images are from maximal projections. (**B**) Protein levels in total lysate (T), 13,000×***g*** supernatant (S13) and 13,000×***g*** pellet (P13) fractions were analyzed by immunoblotting using antibodies to mCherry and the ER protein Kar2. The 13,000×***g*** pellet fractions were resuspended in buffer alone or buffer containing 1 M KCl, 0.1 M Na_2CO_3, 3 M urea or 1% TX-100 and separated into supernatant (S) and pellet (P) fractions. (**C**) Cells expressing proteins as indicated were lysed and the lysates (input) were subjected to pull-down by IgG-Sepharose. Input and pull-down fractions were analyzed by immunoblotting with anti-mCherry, -Cdc48, -Erg6, -Pet10, -Erg1 and -Ayr1 antibodies. (**D**) Yeast strains, as indicated, were grown to log phase in YPD and stained with Bodipy for fluorescence microscopy. LD number (black axis) and size (red axis) are shown. n, the number of cells quantified. Scale bars: 5 μm.

in yeast. Interestingly, Ubxd8 expressed from the *GPD1*, but not the *UBX2* promoter, rescued the LD defect (Fig. 6B) and restored the level of TAG (supplementary material Fig. S3) in *ubx2Δ* cells. This activity is specific for Ubxd8 because other mammalian UBX-domain-containing proteins, such as Ubx1 and ASPL (the closest homolog of yeast Ubx4), failed to rescue the LD defect in *ubx2Δ* cells even when they were expressed under the strong *GPD1* promoter in yeast (Fig. 6A,B). In addition, Ubxd8 expression rescued the degradation defect of CPY*–HA and Deg1–GFP (Fig. 3B), and the slow growth phenotype associated with *ubx2Δ* (Fig. 5C). Similar to Ubx2–GFP, GFP–Ubxd8 expressed in yeast, localized to ER, mitochondria and LDs, although its mitochondrial localization appeared to be more prominent (Fig. 5D). Thus, Ubxd8 probably complements the Ubx2 activities for LD maintenance directly on LDs in *ubx2Δ* cells. Together, these results suggest a functional conservation between Ubx2 and Ubxd8.

Discussion

UBX-domain-containing proteins belong to a class of evolutionarily conserved adaptor proteins for the ubiquitin-selective chaperone Cdc48 (also known as VCP and p97) (Römisch, 2006). The budding yeast *S. cerevisiae* contains seven UBX-domain-containing proteins Ubx1–Ubx7. Their functions are largely unknown, except for Ubx2 that is a well-characterized ERAD protein. During ERAD, Ubx2 links the substrate recognition machinery to the dislocation machinery by use of its UBA domain, which binds ubiquitylated substrates, and its UBX domain, which interacts with the Cdc48–Npl4–Ufd1 complex (Neuber et al., 2005; Schuberth and Buchberger, 2005; Schuberth et al., 2004).

In this study, we have established a previously unidentified role for Ubx2 during LD homeostasis. We found that Ubx2 dynamically localizes to ER, mitochondria and LDs. Interestingly, the LD association of Ubx2 correlated well with the timing of LD formation (Fig. 1). Phenotypic analyses showed that LDs in *ubx2Δ* cells are smaller and heterogeneous (Fig. 2). In addition to aberrant morphology, the composition of LD proteins, including Pet10 and Erg6, in *ubx2Δ* cells was substantially different from that in wild-type cells (Fig. 2E). Because the roles of most LD proteins in LD homeostasis have not been established in yeast, it remains unclear whether the LD morphological defect in *ubx2Δ* cells might be linked to any change in the abundance of LD proteins. Domain analysis results showed that deletion of the UBX and UBA domains in Ubx2 has no apparent effect on LDs (Fig. 3A–C). However, LD morphology was aberrant when both domains were removed from Ubx2 (Fig. 3A–C). Thus, we suspect that the two domains cooperate for Ubx2 functions during LD homeostasis, to coordinate independent events or to maintain proper conformation of Ubx2 on the membranes. When Ubx2 variants were overexpressed in yeast cells, most of them resulted in LD aggregation, except for *ubx2* lacking both UBA and UBX domains (Fig. 3E). Localization results confirmed that LD aggregation correlates with excessive Ubx2 on LDs, whereas smaller and heterogeneous LD phenotype correlates with the exclusion of Ubx2 from LDs (Fig. 3E,F). Therefore, we propose that Ubx2 uses its UBX and UBA domains to control its association with LDs and that the two domains probably work together to select for effectors needed for LD homeostasis. This new function for Ubx2 is independent of ERAD, because the ERAD components did not colocalize with Ubx2 in LDs, and their mutants caused different LD phenotypes from that in *ubx2Δ* cells (supplementary material Fig. S2).

Lipid analysis identified that *ubx2Δ* cells accumulate only 50% of normal cellular TAG (Fig. 4A) and that the reduction of TAG correlates well with the LD defects in various *ubx2* mutants (supplementary material Fig. S3). Because TAG forms the inner core of LDs and is thought to control LD size in yeast (Czabany et al., 2008; Fei et al., 2008; Fei et al., 2011; Sorger et al., 2004); the reduction of TAG explains, at least in part, the reduced LD size in *ubx2Δ* cells. TAG in yeast is converted from DAG, mainly by Dga1 and Lro1 that transfer acyl chains to DAG from acyl-CoA and phospholipids, respectively (Sorger and Daum, 2002). Interestingly, we found that Dga1 and Lro1 associate with LDs in different ways (Fig. 4E). Whereas Dga1 localized to the limiting membranes of LDs, Lro1 was enriched at a unique site on the ER juxtaposed to LDs (Fig. 4F). The Lro1 site is reminiscent of the putative LD assembly site marked by Nem1, a protein that recruits Pah1 to the ER for DAG production (Adeyo et al., 2011). However, our data clearly demonstrated that Lro1 does not colocalize with Nem1, although they both were found next to LDs (Fig. 4F). Thus, Lro1 and Nem1 might define distinct microdomains in the ER for different types or maturation status of LDs. Alternatively, they might be sequentially recruited to the same LD assembly site during LD biogenesis. Our result also revealed that Lro1 was partially colocalized with Fld1, the yeast homolog of mammalian seipin (Fig. 4F) (Fei et al., 2008; Szymanski et al., 2007). This result is expected because Lro1 forms only one visible focus that dynamically associates with one LD at a time, whereas Fld1 is localized to all LD contact sites within the ER (Szymanski et. al., 2007).

The acyltransferases Dga1 and Lro1 catalyze the last step of TAG production, which should be coupled to LD assembly. We provide further evidence that Ubx2 is important for TAG synthesis, through its regulation of Lro1. First, *ubx2Δ* caused Lro1 mislocalization, whereas Dga1 was not affected (Fig. 4G). Second, in cells expressing Lro1 or Dga1 as the sole acyltransferase for production of neutral lipids, *ubx2Δ* caused LD defects only in the cells expressing Lro1 but not those expressing Dga1 (Fig. 5D). We suspect that the mislocalization of Lro1 in *ubx2Δ* cells probably results in TAG synthesis or incorporation defects and/or reduced accessibility of Lro1 to its substrate DAG. Thus, the two TAG-synthesizing enzymes mediate neutral lipid production and LD biogenesis through two independent pathways, with Lro1 requiring Ubx2 but Dga1 does not. Because Ubx2–GFP did not show the same type of dynamics as Lro1–mCherry (Fig. 4F; supplementary material Movie 1) and Ubx2 did not bind Lro1 directly (Fig. 5C), Ubx2 might define an ER subdomain that indirectly allows Lro1 targeting and/or regulates the dynamic movement of Lro1. By localizing to the dynamic foci, Lro1 might control LD assembly by remodeling phospholipids (Dahlqvist et al., 2000; Oelkers et al., 2000), and the locally produced lysophospholipids, together with TAG, might contribute to LD nucleation, formation or expansion. Although Dga1 and Lro1 have a redundant role in synthesizing TAG (Czabany et al., 2008; Sorger and Daum, 2002), *dga1Δ* and *lro1Δ* alone reduced TAG to about half the normal level, similar to *ubx2Δ* (supplementary material Fig. S3). However, the LD size in these two mutants was similar to that in the wild type (supplementary material Fig. S3). Thus, the aberrant LDs in *ubx2Δ* cells were not simply due to the

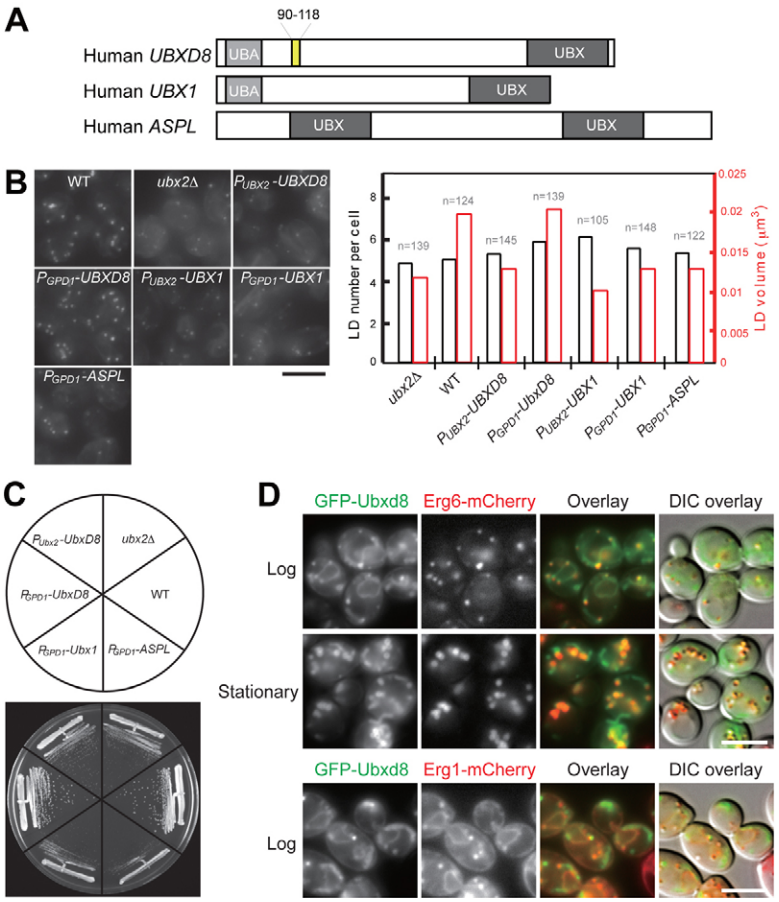

Fig. 6. Mammalian Ubxd8 complements the defects in *ubx2Δ*. (**A**) Diagram of domains and transmembrane regions (yellow) in three human UBX-domain-containing proteins as indicated. (**B**) Left: Wild-type, *ubx2Δ* and *ubx2Δ* cells expressing human Ubx proteins driven by P_{UBX2} or P_{GPD1}, as indicated, were imaged for their LDs at log phase in YPD. Right: The number of LDs (black axis) and size (red axis) are shown. n, the number of cells quantified. (**C**) The indicated strains grown on YPD plate for 2 days were compared. (**D**) Cells expressing GFP–Ubxd8 together with the LD marker Erg6–mCherry or the ER and LD marker Erg1–mCherry were imaged under the growth conditions indicated. Scale bars: 5 μm.

reduced TAG accumulation and Lro1 mislocalization. Similar to its involvement in many types of ERAD, Ubx2 could control several steps of LD homeostasis besides TAG synthesis by Lro1.

LDs are present in virtually all eukaryotic cells and central for lipid homeostasis. We provide evidence that the mammalian Ubxd8 complements the defect of yeast *ubx2Δ* in both ERAD and LD maintenance (Fig. 6). Thus, our results suggest a conserved role of these UBX-domain-containing proteins during evolution. However, Ubxd8 has been shown to inhibit TAG production in fatty-acid-depleted mammalian cells (Lee et al., 2010), which appears to contradict the proposed role of Ubx2 in yeast. The discrepancy might be explained by the dosage effect, as we have found that both depletion and overproduction of Ubx2 cause LD defects (Fig. 3). Ubx2 and Ubxd8 might regulate LD homeostasis by using their UBX and UBA domains to recruit and/or interact with several effectors. During ERAD, these functional domains mediate the interactions between ubiquitylated substrates and ERAD dislocation complex for subsequent proteasomal degradation. These domains could also couple to regulators for lipid homeostasis. In a recent report, Ubxd8 was found to alter its structure in response to unsaturated fatty acids (Lee et al., 2010). Like Ubxd8, Ubx2 might undergo conformational change in response to fatty acids levels during diauxic shift and in the stationary phase. Upon the conformational change, Ubx2 and Ubxd8 might prefer lipid monolayer than lipid bilayer, resulting in LD localization. A versatile protein like Ubx2 (Ubxd8) might then couple the conformational change to exclude interactions with a subset of substrates and promote interactions with another sets of substrates including those involved in lipid synthesis and transport. Thus, identification of Ubx2 substrates on LDs is necessary to understand the mechanisms involved in Ubx2 (Ubxd8) control of LD homeostasis.

The biogenesis and regression of LDs are fundamental cellular processes. Although the biochemical steps of lipid metabolism have been studied extensively, how these biochemical events are coupled to the structure and functions of LDs is largely unknown. Our studies on the UBX-domain-containing proteins reveal an evolutionarily conserved mechanism that links lipid synthesis to the lipid storage organelle.

Materials and Methods

Reagents

Restriction and modifying enzymes and the PageSilver TM silver staining kit were from Thermo Fisher Scientific, Inc.; lipids were from Avanti; Bodipy 493/503, oligonucleotides and the cDNA of HeLa cells used for *UBXD8* cloning were from Invitrogen; the human *UBX1* and *ASPL* cDNA clones were from Thermo; Complete EDTA-free protease inhibitor cocktails were from Roche; and all other reagents were from Sigma-Aldrich. Anti-Ubx2, anti-Erg1, anti-Erg6, anti-Ayr1, anti-Pet10 and anti-mCherry antibodies were raised in rabbits using recombinant Maltose-binding protein (MBP)–Ubx2, MBP–Erg1, MBP–Erg6, MBP–Ayr1, MBP–Pet10 and 6XHis–mCherry as antigens, respectively. Anti-Kar2 antibody was from the Randy Schekman laboratory (UC Berkeley, CA), anti-Cdc48 was from the Rey-Huei Chen laboratory (IMB, Academia Sinica, Taiwan) and anti-GFP antibody was affinity-purified in our laboratory. Anti-HA and anti-Myc antibodies were from Covance; anti-actin antibody was from Millipore and anti-protein-A antibody was from Jackson ImmunoResearch. All DNA sequencing was performed by the core laboratory at Academia Sinica.

Yeast strains and growth conditions

All yeast strains and plasmids used in this study are listed in supplementary material Fig. S1. To generate strains expressing *ubx2* variants, we used the pRS305 cassette described in supplementary material Fig. S1. For other yeast strains, a PCR-based transformation method was used (Longtine et al., 1998). We always started experiments with freshly streaked cells on yeast-extract–peptone–dextrose (YPD) medium from glycerol stocks. Fresh colonies were grown in YPD (2% peptone, 1% yeast extract and 2% glucose) at 30℃ overnight. The medium was refreshed and cells were grown in conditions indicated in the text. The log-phase growth is defined as OD=2.0 in YPD and OD=0.6–0.8 in SCD (0.67% yeast nitrogen base, amino acids and 2% glucose), and the diauxic shift growth was determined from the growth curve of the cells. To shift from 30℃ to 37℃, log-phase cells were diluted in an equal volume of pre-warmed medium and incubated at 37℃ for 1 hour.

Cells were stained with Bodipy 493/503 (0.1 μg/ml) in the dark for 10 minutes, washed twice with 50 mM Tris-HCl (pH 7.5) and immediately subjected to microscopy. Z-section images of nine optical sections spaced at 0.6 μm were captured using a CoolSNAP^{TM} HQ^2 CCD camera (Photomotrics) attached to an Olympus IX81 fluorescence microscope with a GFP filter and a 100× objective lens (NA=1.4). Image capture, deconvolution and projection were performed with analysis LS professional software (Olympus). For still images, cells were either captured using the DeltaVision system (Applied Precision, Inc.) with a 100× objective lens (NA=1.4) and a CoolSNAP^{TM} HQ^2 CCD camera (Photomotrics) controlled by SoftWorx Suite (Applied Precision, Inc) or the Olympus IX81 microscopes described above. To determine Lro1–mCherry colocalization with endomembrane markers, we took Z-section images using the DeltaVision system. Images were processed by deconvolution and maximal projection. The same system was also used for the detection of Lro1–mCherry dynamics by time-lapse microscopy. Images were taken every 20 seconds for 3 minutes. The GFP (525/50) and mCherry (632/60) filter set of SSI7 color solid state illumination system was used with the DeltaVision system. The filter for GFP (excitation: HQ470/40x; emission: HQ525/50m) and mCherry (excitation: HQ575/50x; emission: HQ640/50m) was used with the Olympus IX81 microscope. Images were processed using Adobe Photoshop software.

Transmission electron microscopy

Yeast cells were frozen using a Leica EMPACT2 freezer at a pressure of 2000–2050 bar. Freeze substitution in anhydrous acetone containing 1% OsO_4 and 0.1% uranyl acetate was performed using a Leica EM AFS2 system. The samples were kept at −85℃ for 3 days, followed by one day each at −60℃, −20℃, 0℃ and then room temperature. After rinsing twice with acetone for 12 hours each and twice with propylene oxide for 4 hours each, Spurr's resin was applied for infiltration and embedding. Ultrathin sections (70–90 nm) were prepared using the Reichert Ultracut S or Lecia EM UC6 (Leica, Vienna, Austria). The sections on 100 mesh copper grids were stained with 5% uranyl acetate in 50% methanol for 10 minutes, followed by 0.4% lead citrate for 4 minutes. Sections were observed using a Philips CM 100 transmission electron microscope at 80 kV and images were captured using a Gatan Orius CCD camera.

LD quantification

Metamorph 'granularity' module was used to quantify the diameter and number of LDs. Briefly, fluorescence images were first set to the same brightness and contrast range and the same minimum and width settings to perform analyses using the imaging software. The Metamorph tool 'manually count objects' was used to calculate number of cells in DIC images. Mother cells were counted as 1 and daughter cells, regardless of size, were counted as 0.5. The data were imported into Excel for statistical analysis or presented as scatter plot using GraphPad Prism 4 software (GraphPad Software, Inc).

LD purification and analyses

LDs were isolated from a 1 l culture grown in SCD to OD=1.6 using procedures described previously (Leber et al., 1994) with a few modifications. Briefly, cells were converted to spheroplasts and dounce homogenized in buffer A [10 mM Tris-HCl, pH 6.9, 0.2 mM EDTA and 12% (w/w) Ficoll] with addition of protease inhibitor cocktail, and overlaid with an equal volume of buffer A in a centrifuge tube (Beckman SW41). After centrifugation at 14,000 ***g*** at 4℃ for 1 hour, the floating layer was collected and resuspended in buffer A and overlaid with an equal volume of buffer B [10 mM Tris-HCl, pH 7.4, 0.2 mM EDTA and 8% (w/w) Ficoll]. After centrifugation, the floating layer was collected and resuspended in buffer C [10 mM Tris-HCl, pH 7.4, 0.2 mM EDTA, 0.6 M sorbitol and 8% (w/w) Ficoll] and overlaid with an equal volume of buffer D (10 mM Tris-HCl, pH 7.4, 0.2 mM EDTA and 0.25 M sorbitol) for another centrifugation to yield pure LDs. Equal amounts of pure LDs were resuspended in MURB (50 mM sodium phosphate, 25 mM MES, pH 7.0, 1% SDS, 3 M urea and 5% β-mercaptoethanol) for SDS-PAGE followed by silver staining and western blotting. Proteins from wild-type (BY4742) LDs were subjected to mass spectrometry followed by protein identification.

Lipid analysis

Lipids were isolated from 250 ml cultures that were grown in YPD to OD=2.0 using Folch's method (Folch et al., 1957) with some modifications. Briefly, cells were resuspended in chloroform:methanol (2:1) and lysed with liquid nitrogen. A salt solution (0.04% $CaCl_2$, 0.034% $MgCl_2$, 0.58% NaCl and 0.74% KCl) was added to separate lipids into the organic phase. Lipids were then dried with a BUCHI Rotavapor II and dissolved in 500 μl chloroform. For thin layer chromatography, lipids were applied to a silica gel 60 plate as described previously (Leber et al., 1994) using the solvent systems of light petroleum:diethyl ether:acetic acid (25:25:1) followed by light petroleum:diethyl ether (49:1). Lipids were stained with a $MnCl_2$ solution and heated at 170℃ for ~10 minutes. Standards, including glyceryl trioleate for TAG, cholesteryl stearate for SE, and pure ergosterol and DAG were used to quantify lipids by determining the band intensity using the UVP VisionWorks LS software.

Subcellular fractionation and membrane biochemistry assays

The cell walls were removed form yeast cells to obtain spheroplasts which were osmotically lysed in 20 mM HEPES pH 7.4, 150 mM KCl, 250 mM sorbitol, 1 mM $MgCl_2$, 1× protease inhibitor cocktail and 1 mM phenylmethylsulfonyl fluoride. After a pre-clear centrifugation step at 800 ***g*** for 1 minute to remove the cell debris, the total cell lysate (T) was then subjected to centrifugation at 13,000 ***g*** for 10 minutes at 4℃, resulting in the soluble (S13) and pellet (P13) fractions. The P13 pellet fraction was collected and resuspended in lysis buffer containing: 1 M KCl, 0.1 M Na_2CO_3 (pH 10.5), 3 M urea, 1% Triton X-100. After incubation on ice for 20 minutes, all samples were separated into supernatant (S) and pellet (P) fractions by centrifugation at 13,000 ***g*** for 10 minutes. The samples were precipitated with trichloroacetic acid and washed twice with acetone, followed by immunoblot analyses.

A pull-down assay

Cells were grown in SCD to diauxic shift and 20 ml samples were collected and washed in 20 mM NaN_3 for 10 minutes on ice. Cells were subjected to glass-bead lysis in lysis buffer containing 20 mM HEPES, 7.4, 150 mM KCl, 250 mM sorbitol, 1 mM $MgCl_2$, 10 mM *n*-ethylmaleimide, 0.5% Triton X-100, 1× protease inhibitor cocktail and 1 mM phenylmethylsulfonyl fluoride. The cell lysate was first cleared by centrifugation at 13,000 ***g*** for 10 minutes and the supernatant was incubated with 40 μl IgG Sepharose 6 FF beads at 4℃ for 4 hours. Beads were washed four times in 1 ml lysis buffer. Bound proteins were resuspended in 120 μl MURB and boiled for 5 minutes. 10 μl samples were subjected to SDS-PAGE followed by immunoblot analyses.

Acknowledgements

We thank Rey-Huei Chen (IMB, Academia Sinica, Taipei, Taiwan) for sharing lab resources, providing scientific input and critical reading of the manuscript. We are grateful to Benedikt Westermann (Universität Bayreuth, Germany) for sharing the Su9 vectors, Wann-Neng Jane (IPMB Cell Biology Core Laboratory, Academia Sinica) for help with thin-section EM, Mei-Jane Fang for help with imaging quantification and Tuan-Nan Wen (IPMB Proteomic Core Laboratory, Academia Sinica) for help with LD protein identification.

Funding

This study was funded by Academia Sinica and the National Science Council, Taiwan [grant number 96-2311B-001-042- to C.-W. W].

Supplementary material available online at
http://jcs.biologists.org/lookup/suppl/doi:10.1242/jcs.100230/-/DC1

References

Adeyo, O., Horn, P. J., Lee, S., Binns, D. D., Chandrahas, A., Chapman, K. D. and Goodman, J. M. (2011). The yeast lipin orthologue Pah1p is important for biogenesis of lipid droplets. *J. Cell Biol.* **192**, 1043-1055.

Athenstaedt, K., Zweytick, D., Jandrositz, A., Kohlwein, S. D. and Daum, G. (1999). Identification and characterization of major lipid particle proteins of the yeast Saccharomyces cerevisiae. *J. Bacteriol.* **181**, 6441-6448.

Beller, M., Riedel, D., Jänsch, L., Dieterich, G., Wehland, J., Jäckle, H. and Kühnlein, R. P. (2006). Characterization of the Drosophila lipid droplet subproteome. *Mol. Cell. Proteomics* **5**, 1082-1094.

Beller, M., Sztalryd, C., Southall, N., Bell, M., Jäckle, H., Auld, D. S. and Oliver, B. (2008). COPI complex is a regulator of lipid homeostasis. *PLoS Biol.* **6**, e292.

Blanchette-Mackie, E. J., Dwyer, N. K., Barber, T., Coxey, R. A., Takeda, T., Rondinone, C. M., Theodorakis, J. L., Greenberg, A. S. and Londos, C. (1995). Perilipin is located on the surface layer of intracellular lipid droplets in adipocytes. *J. Lipid Res.* **36**, 1211-1226.

Brasaemle, D. L., Dolios, G., Shapiro, L. and Wang, R. (2004). Proteomic analysis of proteins associated with lipid droplets of basal and lipolytically stimulated 3T3-L1 adipocytes. *J. Biol. Chem.* **279**, 46835-46842.

Czabany, T., Wagner, A., Zweytick, D., Lohner, K., Leitner, E., Ingolic, E. and Daum, G. (2008). Structural and biochemical properties of lipid particles from the yeast *Saccharomyces cerevisiae*. *J. Biol. Chem.* **283**, 17065-17074.

Dahlqvist, A., Ståhl, U., Lenman, M., Banas, A., Lee, M., Sandager, L., Ronne, H. and Stymne, S. (2000). Phospholipid:diacylglycerol acyltransferase: an enzyme that catalyzes the acyl-CoA-independent formation of triacylglycerol in yeast and plants. *Proc. Natl. Acad. Sci. USA* **97**, 6487-6492.

Farese, R. V., Jr (1998). Acyl CoA: cholesterol acyltransferase genes and knockout mice. *Curr. Opin. Lipidol.* **9**, 119-123.

Farese, R. V., Jr and Walther, T. C. (2009). Lipid droplets finally get a little R-E-S-P-E-C-T. *Cell* **139**, 855-860.

Fei, W., Shui, G., Gaeta, B., Du, X., Kuerschner, L., Li, P., Brown, A. J., Wenk, M. R., Parton, R. G. and Yang, H. (2008). Fld1p, a functional homologue of human seipin, regulates the size of lipid droplets in yeast. *J. Cell Biol.* **180**, 473-482.

Fei, W., Shui, G., Zhang, Y., Krahmer, N., Ferguson, C., Kapterian, T. S., Lin, R. C., Dawes, I. W., Brown, A. J., Li, P. et al. (2011). A role for phosphatidic acid in the formation of "supersized" lipid droplets. *PLoS Genet.* **7**, e1002201.

Folch, J., Lees, M. and Sloane Stanley, G. H. (1957). A simple method for the isolation and purification of total lipides from animal tissues. *J. Biol. Chem.* **226**, 497-509.

Fujimoto, T., Kogo, H., Ishiguro, K., Tauchi, K. and Nomura, R. (2001). Caveolin-2 is targeted to lipid droplets, a new "membrane domain" in the cell. *J. Cell Biol.* **152**, 1079-1085.

Fujimoto, Y., Itabe, H., Sakai, J., Makita, M., Noda, J., Mori, M., Higashi, Y., Kojima, S. and Takano, T. (2004). Identification of major proteins in the lipid droplet-enriched fraction isolated from the human hepatocyte cell line HuH7. *Biochim. Biophys. Acta* **1644**, 47-59.

Garbarino, J. and Sturley, S. L. (2005). Homoeostatic systems for sterols and other lipids. *Biochem. Soc. Trans.* **33**, 1182-1185.

Goodman, J. M. (2008). The gregarious lipid droplet. *J. Biol. Chem.* **283**, 28005-28009.

Guo, Y., Walther, T. C., Rao, M., Stuurman, N., Goshima, G., Terayama, K., Wong, J. S., Vale, R. D., Walter, P. and Farese, R. V. (2008). Functional genomic screen reveals genes involved in lipid-droplet formation and utilization. *Nature* **453**, 657-661.

Jonas, A. (2000). Lecithin cholesterol acyltransferase. *Biochim. Biophys. Acta* **1529**, 245-256.

Krauss, R. M. (1998). Triglycerides and atherogenic lipoproteins: rationale for lipid management. *Am. J. Med.* **105 Suppl. 1**, 58S-62S.

Leber, R., Zinser, E., Paltauf, F., Daum, G. and Zellnig, G. (1994). Characterization of lipid particles of the yeast, *Saccharomyces cerevisiae*. *Yeast* **10**, 1421-1428.

Lee, J. N., Zhang, X., Feramisco, J. D., Gong, Y. and Ye, J. (2008). Unsaturated fatty acids inhibit proteasomal degradation of Insig-1 at a postubiquitination step. *J. Biol. Chem.* **283**, 33772-33783.

Lee, J. N., Kim, H., Yao, H., Chen, Y., Weng, K. and Ye, J. (2010). Identification of Ubxd8 protein as a sensor for unsaturated fatty acids and regulator of triglyceride synthesis. *Proc. Natl. Acad. Sci. USA* **107**, 21424-21429.

Londos, C., Sztalryd, C., Tansey, J. T. and Kimmel, A. R. (2005). Role of PAT proteins in lipid metabolism. *Biochimie* **87**, 45-49.

Longtine, M. S., McKenzie, A., 3rd, Demarini, D. J., Shah, N. G., Wach, A., Brachat, A., Philippsen, P. and Pringle, J. R. (1998). Additional modules for versatile and economical PCR-based gene deletion and modification in *Saccharomyces cerevisiae*. *Yeast* **14**, 953-961.

Mueller, B., Klemm, E. J., Spooner, E., Claessen, J. H. and Ploegh, H. L. (2008). SEL1L nucleates a protein complex required for dislocation of misfolded glycoproteins. *Proc. Natl. Acad. Sci. USA* **105**, 12325-12330.

Neuber, O., Jarosch, E., Volkwein, C., Walter, J. and Sommer, T. (2005). Ubx2 links the Cdc48 complex to ER-associated protein degradation. *Nat. Cell Biol.* **7**, 993-998.

Novikoff, A. B., Novikoff, P. M., Rosen, O. M. and Rubin, C. S. (1980). Organelle relationships in cultured 3T3-L1 preadipocytes. *J. Cell Biol.* **87**, 180-196.

Oelkers, P., Behari, A., Cromley, D., Billheimer, J. T. and Sturley, S. L. (1998). Characterization of two human genes encoding acyl coenzyme A:cholesterol acyltransferase-related enzymes. *J. Biol. Chem.* **273**, 26765-26771.

Oelkers, P., Tinkelenberg, A., Erdeniz, N., Cromley, D., Billheimer, J. T. and Sturley, S. L. (2000). A lecithin cholesterol acyltransferase-like gene mediates diacylglycerol esterification in yeast. *J. Biol. Chem.* **275**, 15609-15612.

Rajakumari, S., Grillitsch, K. and Daum, G. (2008). Synthesis and turnover of non-polar lipids in yeast. *Prog. Lipid Res.* **47**, 157-171.

Römisch, K. (2006). Cdc48p is UBX-linked to ER ubiquitin ligases. *Trends Biochem. Sci.* **31**, 24-25.

Schuberth, C. and Buchberger, A. (2005). Membrane-bound Ubx2 recruits Cdc48 to ubiquitin ligases and their substrates to ensure efficient ER-associated protein degradation. *Nat. Cell Biol.* **7**, 999-1006.

Schuberth, C., Richly, H., Rumpf, S. and Buchberger, A. (2004). Shp1 and Ubx2 are adaptors of Cdc48 involved in ubiquitin-dependent protein degradation. *EMBO Rep.* **5**, 818-824.

Sorger, D. and Daum, G. (2002). Synthesis of triacylglycerols by the acyl-coenzyme A:diacyl-glycerol acyltransferase Dga1p in lipid particles of the yeast Saccharomyces cerevisiae. *J. Bacteriol.* **184**, 519-524.

Sorger, D., Athenstaedt, K., Hrastnik, C. and Daum, G. (2004). A yeast strain lacking lipid particles bears a defect in ergosterol formation. *J. Biol. Chem.* **279**, 31190-31196.

Stone, S. J., Levin, M. C., Zhou, P., Han, J., Walther, T. C. and Farese, R. V., Jr (2009). The endoplasmic reticulum enzyme DGAT2 is found in mitochondria-associated membranes and has a mitochondrial targeting signal that promotes its association with mitochondria. *J. Biol. Chem.* **284**, 5352-5361.

Sztalryd, C., Xu, G., Dorward, H., Tansey, J. T., Contreras, J. A., Kimmel, A. R. and Londos, C. (2003). Perilipin A is essential for the translocation of hormone-sensitive lipase during lipolytic activation. *J. Cell Biol.* **161**, 1093-1103.

Szymanski, K. M., Binns, D., Bartz, R., Grishin, N. V., Li, W.-P., Agarwal, A. K., Garg, A., Anderson, R. G. and Goodman, J. M. (2007). The lipodystrophy protein seipin is found at endoplasmic reticulum lipid droplet junctions and is important for droplet morphology. *Proc. Natl. Acad. Sci. USA* **104**, 20890-20895.

van Meer, G. (2001). Caveolin, cholesterol, and lipid droplets? *J. Cell Biol.* **152**, F29-F34.

Walther, T. C. and Farese, R. V., Jr (2009). The life of lipid droplets. *Biochim. Biophys. Acta* **1791**, 459-466.

Yang, H., Bard, M., Bruner, D. A., Gleeson, A., Deckelbaum, R. J., Aljinovic, G., Pohl, T. M., Rothstein, R. and Sturley, S. L. (1996). Sterol esterification in yeast: a two-gene process. *Science* **272**, 1353-1356.

Yen, C. L., Stone, S. J., Koliwad, S., Harris, C. and Farese, R. V., Jr (2008). Thematic review series: glycerolipids. DGAT enzymes and triacylglycerol biosynthesis. *J. Lipid Res.* **49**, 2283-2301.

Zehmer, J. K., Bartz, R., Liu, P. and Anderson, R. G. (2008). Identification of a novel N-terminal hydrophobic sequence that targets proteins to lipid droplets. *J. Cell Sci.* **121**, 1852-1860.

Zehmer, J. K., Bartz, R., Bisel, B., Liu, P., Seemann, J. and Anderson, R. G. (2009). Targeting sequences of UBXD8 and AAM-B reveal that the ER has a direct role in the emergence and regression of lipid droplets. *J. Cell Sci.* **122**, 3694-3702.